DOI: https://doi.org/10.68732/034d40adb86a73b9

ISBN: 978-9989-2053-6-1

Permeability Estimation Using X-ray CT Based on 3D Digital Rock Core Images

H. J. Je & K. Y. Kim
Korea Maritime & Ocean University, Busan, Republic of Korea
kykim@kmou.ac.kr
0000-0002-4648-7470

Abstract

Fluid flow characteristics in porous media are important in various fields, including reservoir engineering, subsurface hydrology, and geological carbon sequestration, and permeability is a representative hydraulic property used to quantify such flow behavior. In this study, LBM simulations were performed using a CT-based digital core of Bentheimer sandstone, and the causes of permeability overestimation arising from CT resolution limitations and the binarization process were investigated. The uncorrected LBM permeability was 875 mD, about 2.3 times higher than the experimental value of 386 mD. A comparison between CT-based PSD and MIP-based PSD confirmed the presence of micropore regions that could not be directly resolved by CT imaging. To address this limitation, virtual micropores were generated probabilistically and Brinkman resistance was applied to the corresponding regions. As the generated micropore fraction increased, the resistance applied region expanded and the calculated permeability gradually decreased. In particular, the 2.5% virtual micropore case yielded a permeability of 472mD, which was closest to the experimental value. These results suggest that the unresolved resistance effect of microporosity is one of the main causes of permeability overestimation in CT-based LBM simulations, and that virtual micropore–Brinkman correction can be a practical way to improve permeability prediction accuracy.

Keywords

X-ray CT, Digital core, Lattice Boltzmann Method, Permeability, Micropore correction.

1 Introduction

Fluid flow in porous media is important in various fields, including reservoir engineering, subsurface hydrology, and geological carbon sequestration (Bultreys et al. 2016; Soulaine et al. 2016). Permeability is a representative hydraulic property used to quantitatively evaluate how easily fluid can move through porous rock (Gao et al. 2012). However, conventional permeability tests cannot directly capture internal pore structure, connectivity, or dominant flow pathways and repeated experiments may damage samples and increase cost(Blunt 2001; Xiong et al. 2016).

To address these limitations, X-ray CT-based 3D digital core analysis has been widely used because it enables nondestructive reconstruction of pore structure and quantitative flow evaluation(Cnudde and Boone 2013). In addition, CT-based digital core technology offers advantages in terms of rapid analysis, repeatable computation, and multiphysics simulation (Saxena et al. 2017). In particular, the Lattice Boltzmann Method (LBM) is well suited for direct flow simulation in CT-based pore space because binarized voxel images can be directly used as the computational lattice without additional meshing(Rao and Schaefer 2019).

Nevertheless, CT-based digital core analysis still has limitations associated with image resolution and binarization(Ketcham and Carlson, 2001). Low-resolution X-ray CT can capture the porosity of large pores, but may overestimate pore size and connectivity(Jiang et al. 2012; Peng et al. 2012; Yang et al. 2021). As a result, micropores may be omitted or absorbed into adjacent macropores in the CT-based binary structure, leading to flow paths that appear wider and more connected than they actually are. This can cause permeability to be overestimated in LBM simulations (Jivkov et al. 2013; Yi et al. 2017).

In this study, the causes of permeability overestimation in CT-based LBM simulations are analyzed, and a correction method based on virtual micropore generation and Brinkman resistance is proposed. By comparing permeability and flow fields before and after correction, the applicability of the proposed method is evaluated.

2 Materials and methods

2.1 Dataset and image pre-processing

X-ray CT images of Bentheimer sandstone provided by the Digital Porous Media Portal were used in this study. The voxel size of the CT images was 2.25 μm, and the representative computational domain consisted of 400 × 400 × 400 voxels. The porosity and experimental permeability of the sample were 22.4% and 386mD, respectively, and these values were used as reference data for validating the simulation results. The original CT data consisted of multiple two-dimensional grayscale slices, which were stacked in the z-direction to construct a three-dimensional grayscale volume. Otsu thresholding was then applied to distinguish pore and solid phases and a binary digital core was generated (Fig. 1). Otsu's method is a global thresholding technique that automatically selects the threshold that maximizes the difference in gray values between two classes. The resulting binarized pore structure was finally used as the input geometry for the LBM simulations(Otsu 1979).

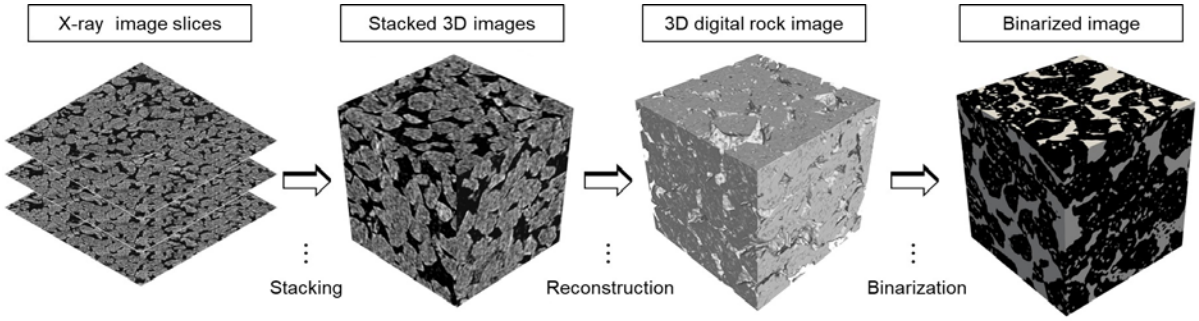


Fig. 1 Workflow for generating the 3D digital core.

2.2 LBM Simulation procedure

LBM simulates fluid flow through the collision and streaming of particle distribution functions on a lattice. In this study, the binarized CT-based digital core was used as the computational domain with each voxel corresponding to one lattice cell. A D3Q19 lattice model and an MRT collision model with an external forcing term were adopted (Xie et al. 2026). The evolution equation of the MRT-based distribution function is given in Eq. (1).

$$f_i(x + e_i\Delta t, t + \Delta t) - f_i(x,t) = -M^{-1}S[m(x,t) - m_i{}^{eq}(x,t)] + F_i (1)$$

In Eq. (1), $f_i(x,t)$ is the density distribution function in the i-th direction at position$x$, and time t, e_i is the D3Q19 discrete velocity vector, M is the transformation matrix, S is the relaxation matrix, $m_i{}^{eq}$ denotes the equilibrium moment,$F_i$represents the external forcing term. In the simulation, a pressure difference was imposed between the inlet and outlet to induce flow in the z-direction, and a bounce-back boundary condition was applied at the solid walls to represent the no-slip condition. The permeability was calculated from the average velocity in the z-direction and the pressure gradient, as shown in Eq. (2).

$$k_{LBM} = \frac{v(u_z)}{\nabla P} (2)$$

where, v is the lattice viscosity, u_z is the average velocity in the z-direction over the entire computational domain, and ∇P is the pressure gradient in the z-direction. The calculated lattice permeability was converted into physical permeability using the voxel size, as given in Eq. (3),

$$k_{phys} = k_{LBM}(\Delta x)^2 (3)$$

where $\Delta x = 2.25 \times 10^{-6} m$. The resulting k_{phys} was then converted into mD and compared with the experimental value.

2.3 Cause of overestimation due to CT resolution limitation

The actual pore network of rock spans a wide range of pore sizes, including many micropores and narrow pore throats smaller than the CT voxel size. However, a CT-based digital core may not fully represent these structures because of the limitations in image resolution and binarization. This limitation can be expressed in two ways. First, when solid and micropores coexist within a single voxel, the averaged gray value may shift toward the solid side, and the voxel is then classified as solid, resulting in the loss of micropore information. Second, if micropores or mixed voxels around macropores are classified as pore, pore boundaries that were originally narrow and discontinuous may be represented as a single continuous large flow channel. In this case, the effective flow path is represented as wider and smoother than it actually is, which leads to permeability overestimation in LBM simulations.

2.4 Virtual micropore generation and Brinkman model

To compensate for the unresolved micropore effect in the CT-based digital core, virtual micropores were additionally defined within the macropore-centered pore structure. Because the exact locations of actual micropores are unknown, virtual micropores were distributed probabilistically within candidate voxels in the computational domain using a random seed (Fig. 2).

Brinkman resistance was then applied to the generated micropore regions. The governing equations of the Brinkman model are given in Eq. (4) and Eq. (5).

$$\nabla \cdot u = 0 (4)$$

$$-\nabla p + \mu_e \nabla^2 u - \frac{\mu}{k_{micro}} u = 0 (5)$$

where u is voxel averaged velocity, p is pressure, μ is the fluid viscosity, μ_e is the effective viscosity, and k_{micro} is the local permeability of the micropore region. The last term represents the resistance

term that suppresses fluid flow in the micropore region. In the LBM implementation, this effect was introduced as an external forcing term, as expressed in Eq. (6).

$$F = -\alpha u (6)$$

In the actual calculation, MRT dynamics with Guo forcing were used, and the force was computed using the pre-force base velocity u_0. As the generated micropore fraction increased, the extent of the Brinkman resistance-applied region also increased, leading to a decrease in the overall permeability of the flow field.

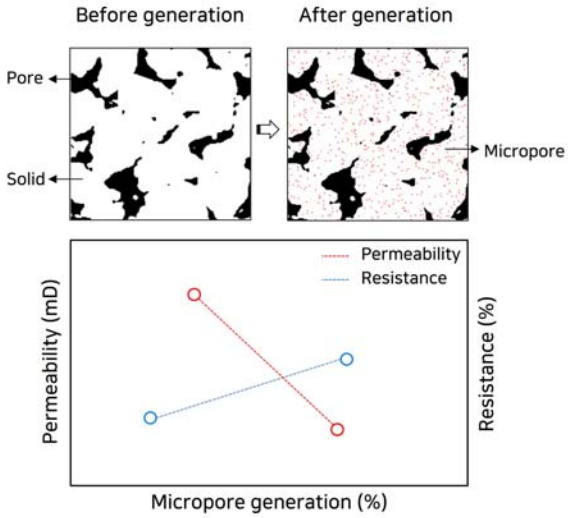


Fig. 2 Visualization of virtual micropore generation.

3 Results

3.1 Uncorrected LBM results and structural limitations of the CT-based digital core

The uncorrected LBM simulation yielded a permeability of 875 mD, which is approximately 2.3 times higher than the experimental value of 386 mD. This suggests that the CT-based binary digital core does not fully represent the actual pore structure. Flow-field visualization also showed that fluid tended to concentrate along a few highly connected large pores rather than passing uniformly through the entire pore network.

To identify the structural cause of this overestimation, the CT-based pore size distribution (PSD) was compared with the mercury intrusion porosimetry (MIP)-based PSD. As shown in Fig. 3, the CT-based PSD is mainly concentrated in the large-pore range of several tens of micrometers, whereas the MIP-based PSD indicates an unresolved micropore region with a significant volumetric contribution in the nanometer range. This provides structural evidence that the CT-based digital core does not sufficiently capture the microporous structure of the actual rock.

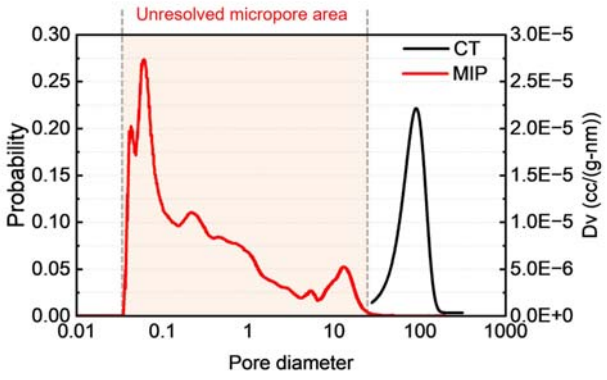


Fig. 3 Comparison between CT-based PSD and MIP-based PSD.

3.2 LBM results and effect of micropore correction

In the LBM simulation using only the CT-based macropore structure, fluid tended to flow preferentially through highly connected large pores, resulting in a simplified flow pathway compared with the actual pore network. To compensate for this limitation, virtual micropores were generated and Brinkman resistance was applied to the corresponding regions, after which the flow field was recalculated. Fig. 4a shows the uncorrected flow field, where the main flow path connecting the inlet and outlet is relatively wide and continuous. In contrast, Fig. 4b shows the corrected case, in which the overall pore geometry is preserved but the dominant flow channel becomes narrower and less continuous. This indicates that the micropore regions acted not as free-flow pore space but as resistive zones that suppressed fluid motion.

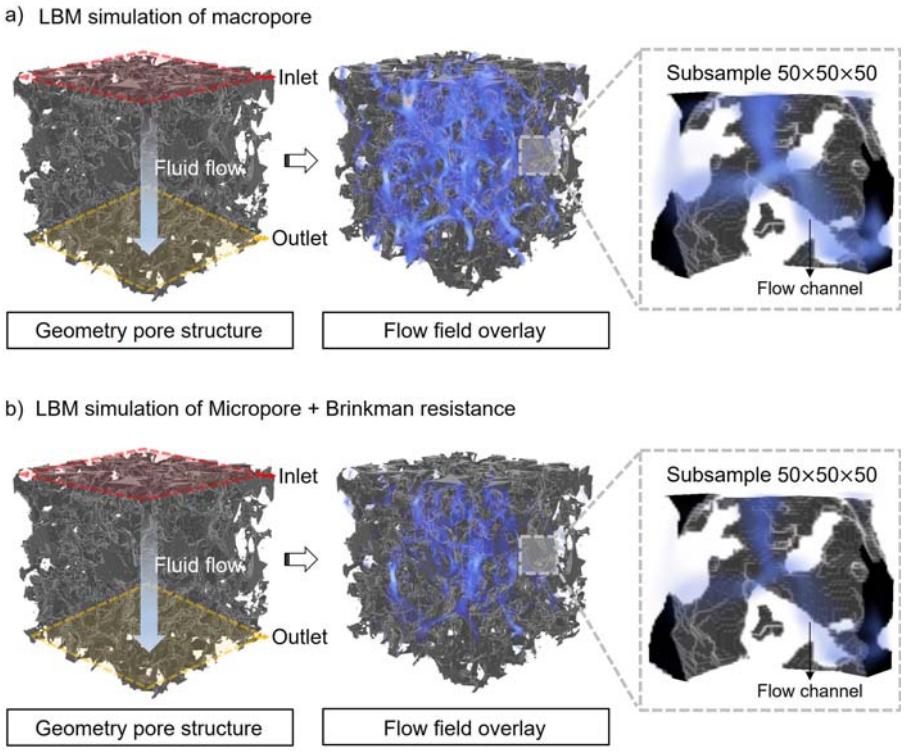


Fig. 4 Comparison of flow fields before and after correction: a)flow field before correction, b)flow field after correction.

Quantitatively, permeability decreased progressively as the generated micropore fraction increased, from 875 mD in the uncorrected case to 792, 713, 628, 537, and 472mD at 0.5%, 1.0%, 1.5%, 2.0%, and 2.5%, respectively (Fig. 5). At the same time, the fraction of the resistance-applied region increased, indicating that a larger portion of the flow domain was subjected to hydraulic resistance. Among the tested cases, the 2.5% virtual micropore condition showed the closest agreement with the experimental value and was therefore considered the most suitable correction condition in this study.

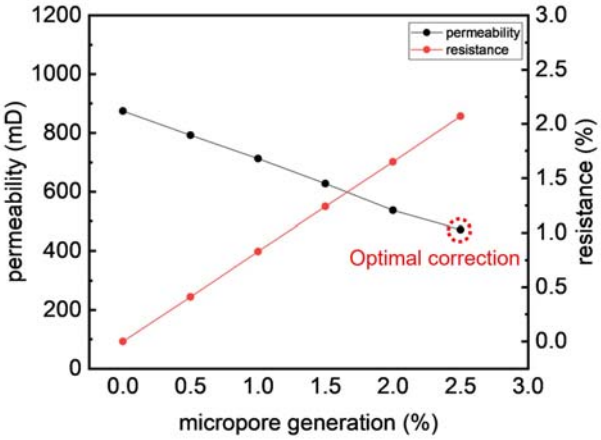


Fig.5 Permeability trend with increasing micropore generation.

3.3 Comparison of experimental, uncorrected and corrected LBM results

The correction effect was evaluated by comparing the experimental permeability, the uncorrected LBM result, and the corrected LBM result. Fig. 6 presents the permeability values for the three cases as a bar chart. The uncorrected LBM result was 875 mD, which is significantly higher than the experimental value of 386 mD, showing that permeability is overestimated when only the CT-based binary digital core is used. In contrast, the corrected LBM result, obtained by introducing virtual micropores and applying Brinkman resistance, decreased to 472mD and showed much closer agreement with the experimental value.

This indicates that micropores below the CT resolution provide additional resistance to fluid flow, and that accounting for this effect can reduce excessively connected flow paths. Therefore, virtual micropore–Brinkman correction is considered an effective method for reducing the overestimation tendency of CT-based LBM simulations. However, because the corrected result does not completely match the experimental value, further calibration of the generated micropore fraction and the Brinkman coefficient is still required.

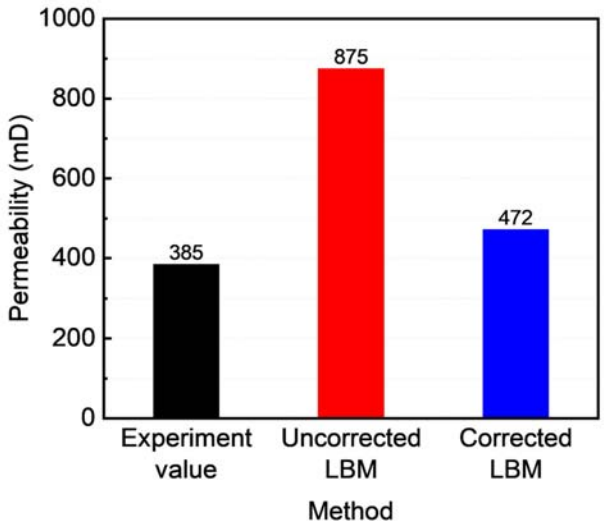


Fig. 6 Comparison of experiment value, uncorrected LBM, and corrected LBM results.

4 Conclusions

In this study, permeability was estimated from a CT-based digital core of Bentheimer sandstone using LBM, and the cause of overestimation associated with CT resolution limitations and binarization was analyzed. The uncorrected LBM result was significantly higher than the experimental value, and the comparison between CT-based PSD and MIP-based PSD confirmed the presence of micropores that could not be directly resolved by CT imaging. To compensate for this limitation, virtual micropores were generated and Brinkman resistance was applied. As the generated micropore fraction increased, the resistance-applied region expanded and the permeability decreased progressively. In particular, the permeability calculated for the 2.5% virtual micropore case showed the closest agreement with the experimental value. These findings suggest that virtual micropore–Brinkman correction is an effective approach for reducing permeability overestimation in CT-based LBM simulations. Future work should focus on improving the physical validity of micropore distribution and systematically calibrating correction parameters for more reliable digital-core-based permeability estimation.

Acknowledgements

This study was supported by the Institute for Korea Spent Nuclear Fuel (iKSNF) (RS-2021-NR056198) and the Busan Metropolitan City grant funded by the Korea government (Ministry of Science and ICT) (A project to support the development of Open-Lab in universities linked to regional industries).

References

Bultreys, T., De Boever, W. and Cnudde, V. (2016) "Imaging and image-based fluid transport modeling at the pore scale in geological materials: A practical introduction to the current state-of-the-art," *Earth-Science Reviews*. Elsevier B.V., pp. 93–128. Available at: https://doi.org/10.1016/j.earscirev.2016.02.001.

Cnudde, V. and Boone, M.N. (2013) "High-resolution X-ray computed tomography in geosciences: A review of the current technology and applications," *Earth-Science Reviews*, pp. 1–17. Available at: https://doi.org/10.1016/j.earscirev.2013.04.003.

Gao, S., Meegoda, J.N. and Hu, L. (2012) "Two methods for pore network of porous media," *International Journal for Numerical and Analytical Methods in Geomechanics*, 36(18), pp. 1954–1970. Available at: https://doi.org/10.1002/nag.1134.

Jiang, Z. *et al.* (2012) "Stochastic Pore Network Generation from 3D Rock Images," *Transport in Porous Media*, 94(2), pp. 571–593. Available at: https://doi.org/10.1007/s11242-011-9792-z.

Jivkov, A.P. *et al.* (2013) "A novel architecture for pore network modelling with applications to permeability of porous media," *Journal of Hydrology*, 486, pp. 246–258. Available at: https://doi.org/10.1016/j.jhydrol.2013.01.045.

Ketcham, R.A. and Carlson, W.D. (2001) "Acquisition, optimization and interpretation of x-ray computed tomographic imagery: Applications to the geosciences," *Computers and Geosciences*, 27(4), pp. 381–400. Available at: https://doi.org/10.1016/S0098-3004(00)00116-3.

Otsu, N. (1979) "A Threshold Selection Method from Gray-Level Histograms," *IEEE Transactions on Systems, Man, and Cybernetics*, SMC-9(1), pp. 62–66.

Peng, S. *et al.* (2012) "Using X-ray computed tomography in pore structure characterization for a Berea sandstone: Resolution effect," *Journal of Hydrology*, 472–473, pp. 254–261. Available at: https://doi.org/10.1016/j.jhydrol.2012.09.034.

Rao, P. and Schaefer, L. (2019) "Lattice Boltzmann models for micro-tomographic pore-spaces," *Computers and Fluids*, 193. Available at: https://doi.org/10.1016/j.compfluid.2019.104294.

Saxena, N. *et al.* (2017) "Effect of image segmentation & voxel size on micro-CT computed effective transport & elastic properties," *Marine and Petroleum Geology*, 86, pp. 972–990. Available at: https://doi.org/10.1016/j.marpetgeo.2017.07.004.

Soulaine, C. *et al.* (2016) "The Impact of Sub-Resolution Porosity of X-ray Microtomography Images on the Permeability," *Transport in Porous Media*, 113(1), pp. 227–243. Available at: https://doi.org/10.1007/s11242-016-0690-2.

Xie, Q. *et al.* (2026) "Pore-Scale Transition Behavior of Digital Carbonate Rock Dissolution During CO2 Geo-Sequestration," *Water Resources Research*, 62(2). Available at: https://doi.org/10.1029/2025WR041604.

Xiong, Q., Baychev, T.G. and Jivkov, A.P. (2016) "Review of pore network modelling of porous media: Experimental characterisations, network constructions and applications to reactive transport," *Journal of Contaminant Hydrology*. Elsevier B.V., pp. 101–117. Available at: https://doi.org/10.1016/j.jconhyd.2016.07.002.

Yang, E., Kang, D.H. and Yun, T.S. (2021) "Ternary segmentation and estimation of permeability for porous rocks based on 3D X-ray computed tomographic images by hidden Markov random field and Brinkman-force lattice Boltzmann model," *Journal of Hydrology*, 599. Available at: https://doi.org/10.1016/j.jhydrol.2021.126377.

Yi, Z. *et al.* (2017) "Pore network extraction from pore space images of various porous media systems," *Water Resources Research*, 53(4), pp. 3424–3445. Available at: https://doi.org/10.1002/2016WR019272.